Volume 12
Number 42
14 November 2020
Pages 21463-21954

Nanoscale

rsc.li/nanoscale

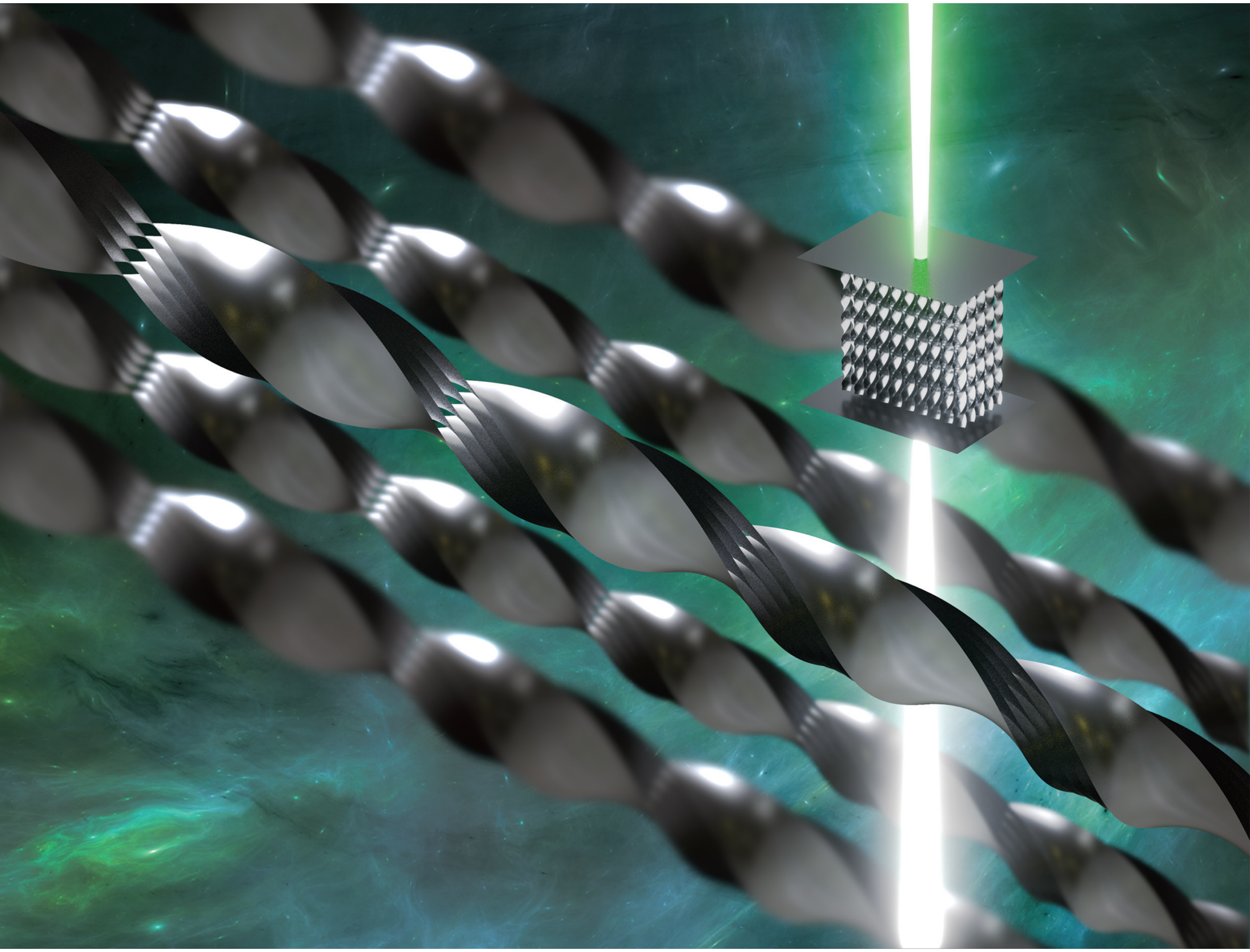

ISSN 2040-3372

ROYAL SOCIETY
OF **CHEMISTRY**

PAPER
Teun-Teun Kim, Dong Ki Yoon *et al.*
Security use of the chiral photonic film made of helical liquid crystal structures

NCNST

Nanoscale

ROYAL SOCIETY OF CHEMISTRY

PAPER

View Article Online
View Journal | View Issue

Cite this: *Nanoscale*, 2020, **12**, 21629

Security use of the chiral photonic film made of helical liquid crystal structures†

Wongi Park,[a] Taewoo Ha,[b,c] Taek Sun Jung,[d] Kyung Ik Sim,[d] Jae Hoon Kim,[d] Joanna M. Wolska,[e] Damian Pociecha,[e] Ewa Gorecka,[e] Teun-Teun Kim*[b,c] and Dong Ki Yoon*[a,f]

Received 14th May 2020,
Accepted 10th July 2020

DOI: 10.1039/d0nr03743e

rsc.li/nanoscale

The color change of photonic crystals (PCs) has been widely studied due to their beauty and anti-counterfeiting applications. Herein, we demonstrated security codes based on chiral PCs that cannot be easily mimicked and are quite different from the conventional technology used currently. The chiral PCs can be made by self-assembly and the structural colors change based on the polarization of the light in the transmission mode. These color changes are easily detected in real-time and are useful in the fabrication of anti-counterfeiting patterns that show beautiful and diverse color changes with rotating polarizers. We believe this can provide a new platform in various security and color-based applications.

Introduction

Photonic crystals (PCs) are now widely used in day-to-day applications such as security, information display, logo patches, smart windows, and sensors and are made of periodically deposited dielectric materials.[1–4] The periodic variation of refractive indices in PCs is the key to control photonic bandgap (PBG), which originates from the forbidden propagation of light over specific wavelengths.[5,6] Thus, there have been enormous efforts in manipulating the structures of dielectric materials to achieve vivid structural coloration that cannot be easily deteriorated by ultraviolet light or staining. Due to this virtue, PCs can be applied in security uses, like anti-counterfeiting patterns in bills.[7] Indeed, varying viewing angles on PCs can dramatically switch reflection colors, known as the iridescent coloration[8] and can be seen in anti-counterfeiting patterns; for example, numbers in bills show different colors at different viewing angles.

However, photonic films in current technology are not difficult to mimic using conventional thin-film processes, such as deposition and spin-coating of dielectric materials.[9,10] In other words, the current anti-counterfeiting pattern is not safe. Therefore, advanced anti-counterfeiting technology is required to avoid imitation and should have additional security functionalities. One of the promising technologies is, using chiral PCs that cannot be easily mimicked by conventional fabrication methods and can show color changes depending on polarization by optical rotation of light. One of the essential optical properties in chiral PCs is the optical rotation by polarization of a linearly polarized light (LPL), also known as optical activity.[11] The optical rotation is mainly caused by circular birefringence, resulting in retardation of the phase of specific circularly polarized light (CPL). In general, LPL is expressed as a combination of two bases of CPL as $E = E_x\hat{x} + E_y\hat{y} = |E_\mathrm{l} + E_\mathrm{r}|\hat{x} - i|\,E_\mathrm{l} - E_\mathrm{r}|\hat{y}$, where E_x and E_y are the linearly polarized electric field strengths along the x- and y-axis, respectively. E_l and E_r are the left and right circularly polarized electric field strengths, respectively. The oscillation direction of LPL is determined by the phase difference between two CPLs, which means that the polarization plane of incident LPL can be rotated by changing the phase difference. For example, when two CPLs enter a chiral medium, one of the CPLs is retarded due to the difference refractive indices for CPLs, also called circular birefringence. As a result, the polarization plane rotates when LPL passes through the chiral medium. Since the chiral media have inherent strong optical activity and are not easily fabricated by conventional top-down lithographic techniques, it can significantly enhance the security usage.

In this study, we realize a chiral PC film using chiral liquid crystal (LC) phases of a cholesteric liquid crystal (CLC) phase and helical nanofilament (HNF) phase that can form chiral

---

[a] *Graduate School of Nanoscience and Technology, Korea Advanced Institute of Science and Technology (KAIST), Daejeon 34141, Republic of Korea. E-mail: nandk@kaist.ac.kr*
[b] *Center for Integrated Nanostructure Physics (CINAP), Institute for Basic Science (IBS), Suwon 16419, Republic of Korea. E-mail: teun2000@gmail.com*
[c] *Sungkyunkwan University, Suwon 16419, Republic of Korea*
[d] *Department of Physics, Yonsei University, Seoul 03722, Republic of Korea*
[e] *Faculty of Chemistry, University of Warsaw, Warsaw, 02-089, Poland*
[f] *Department of Chemistry and KINC, Korea Advanced Institute of Science and Technology (KAIST), Daejeon 34141, Republic of Korea*

† Electronic supplementary information (ESI) available. See DOI: 10.1039/d0nr03743e

1-dimensional (1D) photonic structures by self-assembly.[12–17] In particular, the HNF-based photonic film is robust for practical applications as compared with the CLC-based one. This is a remarkable improvement in this area because it is well known that chiral photonic structures are complicated to fabricate with the top-down lithographic method.[5,18] The resultant achievement can contribute to anti-counterfeiting applications and is more economic than the conventional approaches because of the simple self-assembly process. Previously, many techniques for changing the color of the CLC phase have been developed by controlling temperature,[19] applying an electric field,[20] changing the viewing angle,[8] *etc*. The structural color of CLCs can be easily adjusted with these methods, so they have been examined in various security applications.[21] However, these conventional methods require elaborate experimental set-ups, such as heat controllers or electric field generators. Contrary to previous anti-counterfeiting works, our platform has a unique difference, which is the polarization dependent color change in the transmission mode. Therefore, this system can enhance security functionality because this is only achievable using a chiral PC film.

Results and discussion

Chiral photonic crystals and their fabrication

Generally, 1D PCs (Fig. 1b) made of multi-layered dielectric materials have structural colors in a specific range of wavelengths (λ) based on the Bragg's equation;

$$\lambda = 2nd\cos\alpha, \tag{1}$$

where n is the refractive index, d is the periodic length and α is the angle between the incident light and the PC film. If d is near the hundreds of nanometer scale, certain visible light that matches with eqn (1) is reflected from the PC. This simple 1D structure can be easily made by conventional deposition methods. However, the periodic 1D chiral structure gives additional functionality, such as polarization-dependent transmission color changes due to the optical rotation, and it is also difficult to fabricate (Fig. 1c). When non-chiral and chiral PC films are observed with transmission mode microscopy between two rotatable linear polarizers (Fig. 1a), the polarization-dependent color changes can be observed only in the chiral PC by changing angle θ, as shown in Fig. 1c. Here, θ is the angle between two wire grid linear polarizers (Fig. 1a). In contrast, in the non-chiral film (Fig. 1b), only the brightness is changed. Generally, the intensity of transmitted light from a linear polarizer follows Malus's law, $I = I_0\cos^2\theta$, $I_{0,}$ and I refers to the intensity of light before and after passing through the polarizers. In the non-chiral PC case, which does not have optical rotation, the transmittance intensity (I) is related to $\cos^2\theta$, and this does not depend on the wavelength of light. Therefore, as shown in Fig. 1b, no difference in color and brightness at −70° and +70° is observed. On the other hand, the transmitted LPL passing through the chiral PC film is rotated either clockwise or counterclockwise. Furthermore, the optical rotation is dramatically varied depending on the wavelength due to the different chiral birefringence. As a result, the color is changed by varying the rotation angle θ (Fig. 1c). More details will be discussed in Fig. 4.

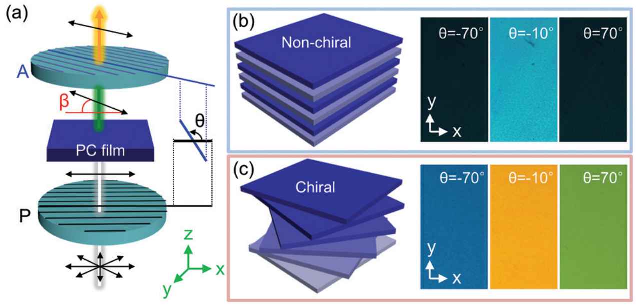

Fig. 1 (a) Experimental set-up of transmission mode with two rotatable linear polarizers. (b) There is no polarization-dependent color change in the non-chiral PC film. Only the brightness is changed. (c) In the chiral PC film, the clear tendency of color change was observed when the polarizer rotates.

It is of note that our resultant system for the anti-counterfeiting code can be generally used even in the reflected color platform. Since our study emphasizes the color changes in a transmission mode that has not been rationalized to date, one might think that the current system is difficult to utilize with a reflective security code. However, the color change of the chiral PC film depends on the viewing angle in reflection mode as well as transmission mode (Fig. S1, ESI†). In the above eqn (1), the reflection color (λ) of a 1D PC is related to the incident viewing angle α. As both the non-chiral and chiral PC films have a 1D structure (Fig. 1b and c), they both have viewing angle-dependent color changes in reflection mode (Fig. S1a, ESI†). However, as the polarization-dependent transmission color change is related to the optical rotation, it only can be observed in the chiral PC film (Fig. S1b, ESI†). Therefore, chiral PC includes not only the characteristic viewing angle dependence of non-chiral PC but also an advanced characteristic.

To determine the chiral characteristics, three kinds of PCs were prepared, including a non-chiral and two chiral structures. (i) A branched nanoporous anodic aluminum oxide (AAO) film was fabricated for a non-chiral 1D structure as previously reported.[22] Since the anodization current changes periodically, nanochannels with periodic air porosity are formed. As the porosity changes periodically, the refractive index also varies. Because of this periodic modulation of the refractive index of AAO (Fig. 2a and Fig. S2, ESI†), AAO forms a 1D non-chiral PC film with 600 nm-PBG. (ii) A cholesteric liquid crystal (CLC) film is prepared for the chiral 1D structure,[11,23] which can be simply made using the nematic host material E7 and chiral dopant S811. Since the molecular director of LC molecules in the CLC phase rotates in a certain period, the CLC material forms periodically stacked layer struc-

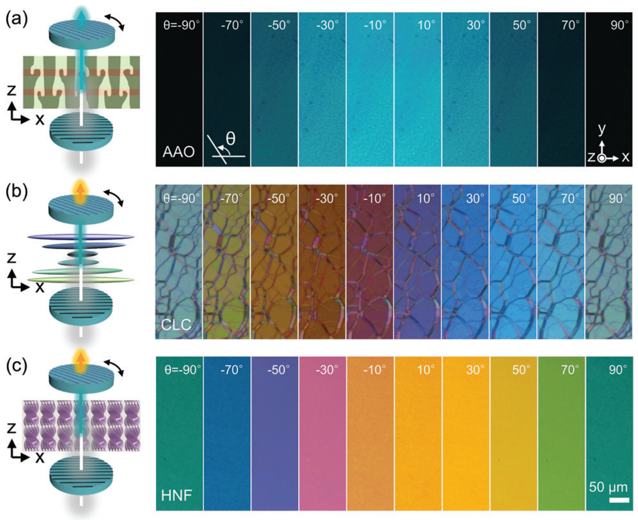

Fig. 2 Experimental comparison of various non-chiral and chiral photonic films with transmission mode. (a) As there is no chiral manner in the branched AAO PC film, only the brightness has been changed when θ rotates. Because of supramolecular chirality in (b) CLC and (c) HNF films, there is a polarization dependence of transmitted light and the color changes accordingly.

tures with a chiral manner (Fig. 2b). As a result, CLC has a PBG determined by a simple equation;

$$\lambda = n_{\text{eff}}p, n_{\text{eff}} = (n_{\text{e}} + n_{\text{o}})/2, \tag{2}$$

where n_{eff}, n_{e}, n_{o}, and p refer to the effective-, extraordinary-, and ordinary refractive indices and helical pitch, respectively. Within the LC cell made of polyimide-coated glass substrates, an oily streak pattern is observed, which demonstrates that the helical axis is aligned in the *z*-axis (Fig. 2b) and has a PBG at 580 nm. (iii) A helical nanofilament (HNF) phase as a chiral PC film was prepared using the photoalignment of azodimer molecule, D-11, as reported previously (Fig. S3, ESI†).[15] In detail, a typical sandwich-type LC cell whose cell gap is maintained at 3 μm with silica beads was used. The dimer molecule D-11 (Fig. S3a, ESI†) was injected into the LC cell by a capillary manner above its isotropic temperature (180 °C). During the cooling process to induce a thermal phase transition into the HNF phase, unpolarized ultraviolet (UV) light is shined onto the sample from a top-to-bottom direction. Initially, LC molecules are randomly distributed before UV irradiation (Fig. S3b, ESI†). However, azobenzene moieties are changed to *cis*-isomers once exposed to UV light (Fig. S3c, ESI†). The molecules tend to change their shapes to their original *trans*-isomer, as the *cis*-state of azobenzene is less stable than the *trans*-state. According to Weigert's effect,[24,25] the polar director of LC molecules rotates toward the light irradiating direction to minimize the light-absorbing efficiency, and eventually LC molecules are photo-aligned. Simultaneously, uniformly aligned HNFs are made due to the thermal phase transition from these aligned molecules (Fig. S3f, ESI†). For comparison, randomly oriented HNFs are formed when HNFs are made without UV irradiation (Fig. S3e, ESI†). It has been reported that the aligned HNFs in the ambient condition have specific electromagnetic coupling due to the densely packed nanostructures, showing a PBG in the visible wavelength region, ~550 nm.[15]

In the given experimental conditions (Fig. 1a and 2a), the brightness of 1D AAO-PC only changes when rotating the polarizer. As mentioned earlier, the same brightness and color are observed regardless of the sign of θ, and the only absolute value of θ can change the brightness. However, CLC-PC and HNF-PC show both brightness and color changes by varying θ (Fig. 2b and c). This clear difference can be explained by the optical rotation of the incident light passing through the chiral medium. CLC and HNF phases have intrinsic chirality due to the twist elastic deformation and saddle splay deformation, respectively.[14,26] Therefore, a chiral PC film has the optical rotation phenomenon, enabled by changes in the polarization state of the light. As a result, the transmitted intensity of the light is also changed according to Malus' law. If we define the optical rotation β after passing through the chiral medium (Fig. 1a), then the polarization state of light rotates to $\theta + \beta$. Therefore, the final Malus' law is modified as followed; $I = I_0 \cos^2(\theta + \beta)$. Since β also varies for each wavelength of light, the transmission color changes, as shown in Fig. 2b and c.

Polarization-dependent optical property of chiral PC film

To further investigate the polarization-dependent color changes, we measured the transmittance of AAO, CLC, and HNF as a function of rotation angle θ from −90° to 90° with a detection range of 400–700 nm (Fig. 3). For AAO-PC (Fig. 3a), the transmittance shows typical linear changes with varying θ along the measured spectrum region as a non-chiral PC film described by the Malus' law. For the chiral PCs, including CLC

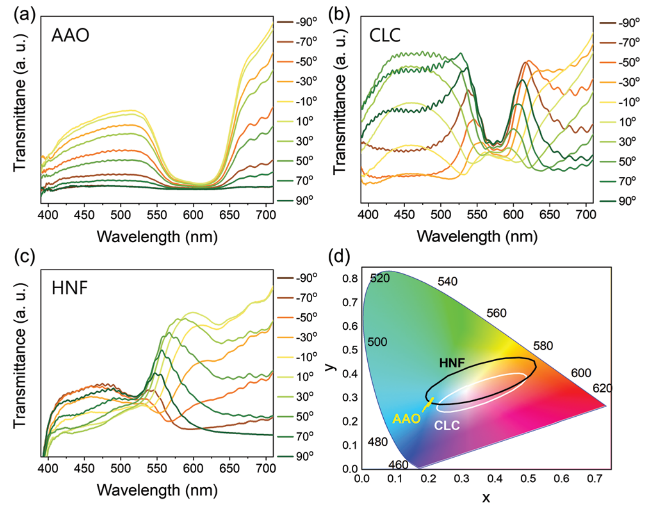

Fig. 3 Spectroscopic investigation of transmittance in (a) AAO, (b) CLC, and (c) HNF film when polarizer rotates. (d) Comparison of color changes of various PCs in a color coordinate chart.

and HNF, the asymmetric transmittance by varying θ is observed, which results in the dramatic changes in colors (Fig. 3b and c). In order to understand the change of the transmission color intuitively, the results of Fig. 3a–c are expressed in the standard color coordinate CIE (Commission internationale de l'éclairage) 1931 color space (Fig. 3d). The polarization angle-resolved color change of 1D-AAO, CLC and HNF PCs in the CIE 1931 color space are marked in yellow, white, and black lines, respectively. While the non-chiral AAO film represents a very small color gamut, the chiral CLC and HNF represent a broad color gamut. In particular, the colors observed in the HNF spans across the red, green, and blue gamut in the CIE chromaticity diagram. Since the light cannot transmit at the PBG, the location of the polarization-selective PBG is important for the color valence in practical applications. Although the CLC has clear polarization-dependent asymmetric transmittance (Fig. 3b), the tunability of the polarization-dependent transmittance around 550 nm (green color) is small due to the location of the PBG. For the HNF, the PBG located below 550 nm (Fig. 3c) leads to a relatively larger color gamut than the CLC. However, the HNF structure is somewhat insufficient for expressing the blue color region due to the weak transmission at 400 nm (blue color), which is closely related to the weak circular dichroism of the intrinsic chirality of molecules below 425 nm (Fig. S4, ESI†). Here, L-HNF and R-HNF refer to each filament twisted in different directions. Since the twisting of HNF occurs randomly, both types of filaments are obtained.[14] Interestingly, the highest transmittance in chiral PC films is not at $\theta = 0$, which does not follow the conventional Malus' law. The representative transmittance change can be found in three wavelength regions, 400 nm, 550 nm, and 700 nm (Fig. 3b and c). The maximum transmittance of HNF-PC at 400 nm, 550 nm, and 700 nm is observed at $\theta = -50°$, $-90°$, and $-10°$, respectively. The optical rotation β can be measured by collecting the θ at the maximum transmittance, which results from the coupling effect between electric and magnetic fields (Fig. 4a and e and Fig. S5, ESI†). β due to chirality follows the formula as

$$\beta = \frac{1}{2}[\arg(T_\mathrm{L}) - \arg(T_\mathrm{R})] = \mathrm{Re}(k)k_0 l \tag{3}$$

where, T_L and T_R are left and right circular transmittance, respectively. k, k_0, and l are the chirality, the wave vector, and the optical path length, respectively. The rotation angle is affected by both k and l. For the sub-micron samples with small l, it is not easy to measure β due to weak k. However, at the flat band in the vicinity of the PBG, light can be drastically slowed down due to strong dispersion, then the effective l is significantly increased.[27] Therefore, enough β is achieved even with a small l of chiral PCs near the PBG (Fig. 4). In the case of CLC (Fig. 4a) and HNF (Fig. 4e), optical rotation suddenly flips over the PBG around $-80°$ to $80°$, which is closely associated with the general anti-resonance effect.[28] For this reason, the optical rotation changes noticeably close to the PBG. At the wavelength of blue (Fig. 4b and f), green (Fig. 4c and g), and red (Fig. 4d and h), different directions and amounts of optical rotation appear. In the case of HNF (Fig. 4f–h), blue and green light have optical rotations of $-60°$ and $+45°$, respectively. However, the red light does not change the polarization plane because of almost no optical rotation. Therefore, rotating the second polarizer in Fig. 1a in the (+) direction makes green light transmittance dominant, and the (−) direction makes blue light transmittance dominant. The ideal angle difference among primary color wavelengths (RGB) for realizing a variety of color is 60°. The rotation angle distribution of HNF is exquisitely close to 60°, which is the original reason for the vivid colors. In contrast, AAO-PC does not have optical rotation due to the lack of chiral structure (Fig. S5, ESI†).

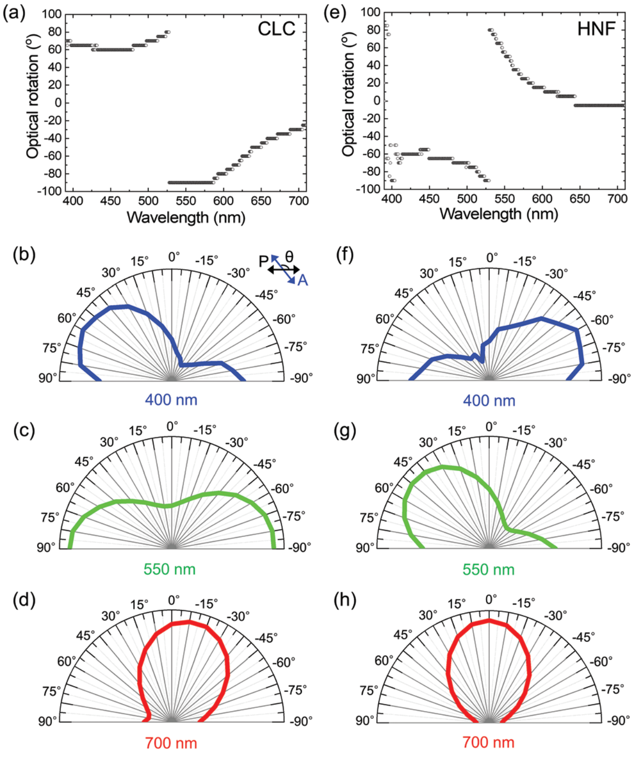

Fig. 4 Wavelength dependent optical rotation in chiral film. The direction and amount of optical rotation are dramatically varied in (a) CLC and (e) HNF films. In each color unit, blue (400 nm), green (550 nm) and red (700 nm), diverse angular anisotropy was observed due to various optical rotation in (b–d) CLC and (f–h) HNF films.

As summarized in Fig. S1,† the chiral PC film not only exhibits viewing angle-dependent color changes in reflection mode (Fig. S1a, ESI†), but also polarization dependency in transmission mode (Fig. S1b, ESI†). As the latter property cannot be realized with the conventional non-chiral PC film, such as a multi-stacked layers or colloidal nanocrystals,[29,30] the suggested chiral system is more comprehensive and advanced for security use. Based on this chiral PC film with new functionality, an anti-counterfeiting tag was realized. For the proof of concept, a micron-scaled mask with intaglio pattern "K" was placed above the HNF-PC film and investigated *via* transmission mode with two polarizers. It was also shown that unique color variation was observed by varying the

Fig. 5 Anti-counterfeiting code made of HNF film. Color variation of security letter "K" in various polarization conditions.

angle θ (Fig. 5). To the best of our knowledge, this is the first demonstration of polarization-dependent color changes of HNF-PC in transmission mode for security applications, even though some of the optical properties have been studied with reflection mode in our previous studies.[11,15]

Conclusions

In summary, the polarization-dependent color variation of the chiral photonic film was studied by comparison between AAO, CLC, and HNF films. Compared to conventional non-chiral PC films, chiral PCs are more difficult to imitate in terms of security applications due to the additional functionality of color variation depending on polarization angle changes. This phenomenon could be understood by the optical rotation in the chiral medium. The optical rotation, the characteristic property of the chiral film, varies dramatically with the wavelength in the vicinity of the PBG, which is associated with a polarization-selective Bragg-type band. The HNF film is quite exquisite in realizing a vivid color level with the appropriate rotation angle difference of about 60° among the main colors of blue, green, and red in the polar map. The various optical rotations are related to the principal mechanism of color changes. As the polarization dependency chirality can only be realized in our chiral PC film, this could reinforce the security functions in PCs.

Experimental

Fabrication of nonchiral PC film

High-purity aluminum foil (99.99%, Alfa Aesar) was first cleaned by acetone, ethanol, and deionized water. The foil was then electrochemically polished at 20 V and 3 °C in an acid solution, which contained perchloric acid and ethanol in a volume ratio of 1 : 5. Pre-anodization was performed at 40 V and 8 °C in a 0.3 M oxalic acid solution. After the chemical etching in a mixture of phosphoric (6 wt%) and chromic (1.8 wt%) acids at 60 °C to selectively remove the anodized alumina remaining well-organized prepattern on the aluminum substrate, additional pre-anodization was performed prior to the pulse anodization in the same condition for 1 hour. After this, pulse anodization with the same oxalic acid solution with periodically controlled currents such as 11 and 2.8 mA cm^{-2} for 24 and 96 s was performed for 200 cycles. Finally, the pore widening process in 0.1 M phosphoric acid solution at 38 °C for 40 min led to vivid structural colors at 600 nm. To investigate the transmission spectrum of this sample, aluminum was selectively removed by a mixture of copper chloride and hydrochloric acid, and a transparent AAO-PC film was obtained.

Fabrication of CLC PC film

To induce the planar-aligned helix of the CLC phase, a planar alignment polyimide (PAPI) was coated on two glass substrates with a spin-coating method and baked for 2 hours at 200 °C. For a typical LC cell, the substrates were attached together with a photo-curable polymer, and its gap was maintained at 3 μm with silica beads. A cholesteric mixture, consisting of nematic host (E7) and chiral dopant (S811) at a 25 wt% concentration, was injected into the LC cell *via* a capillary manner in its isotropic phase. The mixture was cooled slowly to 37.5 °C where its structural color was around 580 nm.

Color coordinate fitting

The colors of our chiral photonic crystals are expressed by a chromaticity diagram in the CIE 1931 color space based on CIE 2° standard observer color matching functions.[31] Our chiral PC's chromaticity is specified by the two derived parameters x and y as follows,

$$x = \frac{X}{X+Y+Z}, y = \frac{Y}{X+Y+Z}$$

using three tristimulus values X, Y, and Z as shown below.

$$\begin{aligned} X &= W^{-1}\int \bar{x}(\lambda)S(\lambda)I(\lambda)\mathrm{d}\lambda, \\ Y &= W^{-1}\int \bar{y}(\lambda)S(\lambda)I(\lambda)\mathrm{d}\lambda, \\ Z &= W^{-1}\int \bar{z}(\lambda)S(\lambda)I(\lambda)\mathrm{d}\lambda. \end{aligned}$$

where $\bar{x}$, $\bar{y}$ and $\bar{z}$ are standard observers about red, green and blue, respectively. W^{-1} is the scaling factor and $S(\lambda)$ is the spectral transmittance of the object being measured, multiplied by the spectral power distribution of the illuminant $I(\lambda)$.

Author contributions

W. P. and T. H. contributed equally to this work. W. P. and D. K. Y. designed the research project; J. M. W., D. P., and E. G. synthesized and performed the initial characterization of dimers; W. P., T. H., T. S. J., K. I. S, and J. H. K. carried out the spectroscopic investigations; W. P., T. H., T.-T. K, and D. K. Y. analyzed the results and wrote the manuscript.

Conflicts of interest

There are no conflicts to declare.

Acknowledgements

This study was supported by a grant from the National Research Foundation (NRF) and funded by the Korean Government (MSIT) (2017R1E1A1A01072798 and 2018R1A5A1025208) and van der Waals Materials Research Center (2017R1A5A1014862). This work was also partially supported by IBS-R011-D1.

References

1 M. Xiao, Z. Hu, Z. Wang, Y. Li, A. D. Tormo, N. L. Thomas, B. Wang, N. C. Gianneschi, M. D. Shawkey and A. Dhinojwala, *Sci. Adv.*, 2017, **3**, e1701151.

2 J.-W. Oh, W.-J. Chung, K. Heo, H.-E. Jin, B. Y. Lee, E. Wang, C. Zueger, W. Wong, J. Meyer, C. Kim, S.-Y. Lee, W.-G. Kim, M. Zemla, M. Auer, A. Hexemer and S.-W. Lee, *Nat. Commun.*, 2014, **5**, 3043.

3 D.-Y. Kim, K. M. Lee, T. J. White and K.-U. Jeong, *NPG Asia Mater.*, 2018, **10**, 1061–1068.

4 M. Pan, L. Wang, S. Dou, J. Zhao, H. Xu, B. Wang, L. Zhang, X. Li, L. Pan and Y. Li, *Crystals*, 2019, **9**, 417.

5 S. Y. Lin, J. G. Fleming, D. L. Hetherington, B. K. Smith, R. Biswas, K. M. Ho, M. M. Sigalas, W. Zubrzycki, S. R. Kurtz and J. Bur, *Nature*, 1998, **394**, 251–253.

6 W. J. Chung, J.-W. Oh, K. Kwak, B. Y. Lee, J. Meyer, E. Wang, A. Hexemer and S.-W. Lee, *Nature*, 2011, **478**, 364–368.

7 H. S. Lee, T. S. Shim, H. Hwang, S.-M. Yang and S.-H. Kim, *Chem. Mater.*, 2013, **25**, 2684–2690.

8 C. Lim, S. Bae, S. M. Jeong and N. Y. Ha, *ACS Appl. Mater. Interfaces*, 2018, **10**, 12060–12065.

9 K. Chung, S. Yu, C.-J. Heo, J. W. Shim, S.-M. Yang, M. G. Han, H.-S. Lee, Y. Jin, S. Y. Lee, N. Park and J. H. Shin, *Adv. Mater.*, 2012, **24**, 2375–2379.

10 P. Lova, G. Manfredi and D. Comoretto, *Adv. Opt. Mater.*, 2018, **6**, 1800730.

11 W. Park, J. M. Wolska, D. Pociecha, E. Gorecka and D. K. Yoon, *Adv. Opt. Mater.*, 2019, **7**, 1901399.

12 H. Wang, H. K. Bisoyi, M. E. McConney, A. M. Urbas, T. J. Bunning and Q. Li, *Adv. Mater.*, 2019, **31**, 1902958.

13 J. Xiang, Y. Li, Q. Li, D. A. Paterson, J. M. D. Storey, C. T. Imrie and O. D. Lavrentovich, *Adv. Mater.*, 2015, **27**, 3014–3018.

14 L. E. Hough, H. T. Jung, D. Kruerke, M. S. Heberling, M. Nakata, C. D. Jones, D. Chen, D. R. Link, J. Zasadzinski, G. Heppke, J. P. Rabe, W. Stocker, E. Korblova, D. M. Walba, M. A. Glaser and N. A. Clark, *Science*, 2009, **325**, 456–460.

15 W. Park, T. Ha, T.-T. Kim, A. Zep, H. Ahn, T. J. Shin, K. I. Sim, T. S. Jung, J. H. Kim, D. Pociecha, E. Gorecka and D. K. Yoon, *NPG Asia Mater.*, 2019, **11**, 45.

16 F. Araoka, G. Sugiyama, K. Ishikawa and H. Takezoe, *Adv. Funct. Mater.*, 2013, **23**, 2701–2707.

17 L. Li, M. Salamonczyk, A. Jakli and T. Hegmann, *Small*, 2016, **12**, 3944–3955.

18 M. Campbell, D. N. Sharp, M. T. Harrison, R. G. Denning and A. J. Turberfield, *Nature*, 2000, **404**, 53–56.

19 P. Zhang, A. J. J. Kragt, A. P. H. J. Schenning, L. T. D. Haan and G. Zhou, *J. Mater. Chem. C*, 2018, **6**, 7184–7187.

20 J. Xiang, A. Varanytsia, F. Minkowski, D. A. Paterson, J. M. D. Storey, C. T. Imrie, O. D. Lavrentovich and P. Palffy-Muhoray, *Proc. Natl. Acad. Sci. U. S. A.*, 2016, **113**, 12925–12928.

21 W. Hong, Z. Yuan and X. Chen, *Small*, 2020, **16**, 1907626.

22 S. H. Ryu, M.-J. Gim, W. Lee, S.-W. Choi and D. K. Yoon, *ACS Appl. Mater. Interfaces*, 2017, **9**, 3186–3191.

23 A. Zep, K. Sitkowska, D. Pociecha and E. Gorecka, *J. Mater. Chem. C*, 2014, **2**, 2323–2327.

24 J.-A. Lv, Y. Liu, J. Wei, E. Chen, L. Qin and Y. Yu, *Nature*, 2016, **537**, 179–184.

25 V. Toshchevikov, T. Petrova and M. Saphiannikova, *Soft Matter*, 2017, **13**, 2823–2835.

26 Z. Zheng, Y. Li, H. K. Bisoyi, L. Wang, T. J. Bunning and Q. Li, *Nature*, 2016, **531**, 352–356.

27 T. Baba, *Nat. Photonics*, 2008, **2**, 465–473.

28 A. V. Kondratov, M. V. Gorkunov, A. N. Darinskii, R. V. Gainutdinov, O. Y. Rogov, A. A. Ezhov and V. V. Artemov, *Phys. Rev. B*, 2016, **93**, 195418.

29 D.-P. Song, C. Li, N. S. Colella, X. Lu, J.-H. Lee and J. J. Watkins, *Adv. Opt. Mater.*, 2015, **3**, 1169–1175.

30 A. V. Blaaderen, R. Ruel and P. Wiltzius, *Nature*, 1997, **385**, 321–323.

31 A. K. R. Choudhury, *Principles of colour and appearance measurement: Object appearance, colour perception and instrumental measurement*, Elsevier, 2014.